

Consortium Members



ESA Cryosat Plus for Oceans

Product Validation Report of the RADS RDSAR processing for oceans (PVR)

Reference: [Cliquez ici pour taper du texte.](#)

Nomenclature: CP40-PVR-RADS-RDSAR

Issue: 1. 0

Date: Jul. 22, 14

M. Naeije

R.Scharroo

Chronology Issues:

Issue:	Date:	Reason for change:	Author
1.0	22/07/14	Creation of PVR Issue 1.0	M. Naeije R. Scharroo

People involved in this issue:

Written by:	M. Naeije (TUDelft) R. Scharroo (EUMETSAT)	2014-07-22
Checked by:	R. Scharroo (EUMETSAT) D. Cotton (SATOC)	
Approved by:	D. Cotton (SATOC)	
Authorized by:		

Distribution:

Company	Means of distribution	Names

List of tables and figures

List of tables:

Table 3-1: Crossover statistics for CryoSat-2 (CS) retracked SLA, SWH and sigma0 with the Jason-1 data (JS1) and Jason-2 data (JS2).	15
---	-----------

List of figures:

Figure 2-1: The different operating modes of the Cryosat-2 SIRAL altimeter	3
Figure 2-2: Overview of constructing the 20Hz PLRM waveform from 4 bursts of 64 echoes.	4
Figure 2-3: Tailor-made hybrid sea state bias model. Left: direct method, sea level anomalies in sigma0-SWH space. Right: Fitted BM4 model with blended in residuals.	5
Figure 3-1: Observation of low wave heights limited by Nyquist frequency of 160 Mhz: square magnitude should increase to 320 MHz (2 times Nyquist).	7
Figure 3-2: Increasing waveform samples from 128 to 256 using technique after Jensen (1999) captures leading edge better.	8
Figure 3-3: Retracking over St. Helana box. Jensen sampling applied.	8
Figure 3-4: Retracking over St. Helena box, noise reduction by $\frac{1}{4} + \frac{1}{2} + \frac{1}{4}$ waveform averaging	9
Figure 3-5: Cryosat-2 standard deviation in sea level: LRM and PLRM combined.	9
Figure 3-6: Jason-1/2 standard deviation in sea level.	10
Figure 3-7: Standard deviation as function of SWH for LRM (left) and PLRM (right).	10
Figure 3-8: CryoSat-2 SLA from PLRM and LRM combined.	11
Figure 3-9: SLA zoomed in on central East Pacific and Northeast Atlantic.	11
Figure 3-10: CryoSat-2 SWH from PLRM and LRM combined.	12
Figure 3-11: CryoSat sigma0 from PLRM and LRM combined.	12
Figure 3-12: Scatterplot CryoSat-2 SWH LRM (left) and PLRM (right) with Jason-2 SWH at crossovers $\Delta t < 5$ days.	13
Figure 3-13: Scatterplot CryoSat-2 sigma0 LRM (left) and PLRM (right) with Jason-2 sigma0 at crossovers $\Delta t < 5$ days.	13
Figure 3-14: CryoSat-2 retracked sea level (SLA) crossover differences. From left to right and from top to bottom: RMS with Jason-1, Jason-2, and Jason-1 with Jason-2, and mean with Jason-1, Jason-2, and Jason-1 with Jason-2.	14
Figure 3-15: CryoSat-2 retracked SWH and sigma0 crossover differences. From left to right and from top to bottom: RMS SWH with Jason-1, Jason-2, and Jason-1 with Jason-2, and RMS sigma0 with Jason-1, Jason-2, and Jason-1 with Jason-2.	15
Figure 3-16: Time series of sea level anomaly (top) and SLA single-satellite crossover differences (bottom), Cryosat-2 LRM only (left) and PLRM only (right).	16
Figure 3-17: Time series of significant wave height (top) and SWH single-satellite crossover differences (bottom), Cryosat-2 LRM only (left) and PLRM only (right).	16
Figure 3-18: Time series of sigma0 (top) and sigma0 single-satellite crossover differences (bottom), Cryosat-2 LRM only (left) and PLRM only (right).	17
Figure 4-1: Evolution of global mean sea level including all historic altimeter data available in RADS. The CryoSat-2 result seamlessly fit the earlier and simultaneous data.	18

Reference documents

RD 1 Algorithm Theoretical Basis Document (ATBD) of the RADS RDSAR processing for oceans
TUD-RDSAR-ATBD-V0.2

Acronyms List

AIR	Azimuth Impulse Response
ATBD	Algorithm Theoretical Basis Document
BRF	Burst Repetition Frequency
CAL2	Calibration mode 2
CP40	Cryosat Plus for Oceans
EO	Earth Observation
ESA	European Space Agency
FBR	Full Bit Rate (un-calibrated, geo-located I and Q individual echoes in time domain)
FFT	Fast Fourier Transform
FSSR	Flat Sea Surface Response
I/Q	In-phase (real) and Quadrature (imaginary)
IPFDB	Instrument Processing Facility Data Base
L1A	Level 1A
L1B	Level 1B
L2	Level 2
LPF	Low-pass filter
LRM	Low Resolution Mode
LSE	Least Squares Estimator
NRT	Near Real Time
PLRM	Pseudo Low Resolution Mode
POD	Precise Orbit Determination
PTR	Point Target Response
PVR	Plan Validation Report
RDSAR	Reduced Synthetic Aperture radar
RIR	Range Impulse Response
SAR	Synthetic Aperture radar
SIRAL	Sar Interferometric Radar ALtimeter
SLA	Sea level Anomaly
SSB	Sea State Bias
SWH	Significant Wave Height

List of Contents

1. Introduction	1
1.1. Purpose and scope	1
1.2. Document structure.....	1
2. Data and method overview	3
2.1. Selection of data areas	3
2.2. Data processing methodology	4
2.2.1. Retracking of Cryosat-2 (P)LRM waveforms.....	4
2.2.2. Incorporating Cryosat-2 data into RADS	4
2.2.3. RADS data selection	5
3. Validation results and overall assessment.....	7
3.1. LRM - SAR - LRM transition.....	7
3.2. Global plots of combined LRM and PLRM	9
3.3. Crossover differences	13
3.4. Long-term evolution of range bias and crossover difference	16
4. Conclusion	18
5. References	20

1. Introduction

1.1. Purpose and scope

This document covers the Plan Validation Report (PVR) for the CryoSat-2 RDSAR L2 product over the oceans generated from the Radar Altimeter Database System RADS by Altimetrics/NOAA/TU Delft in frame of the Cryosat Plus for Oceans project (CP40). We report on the validation results and error analyses of these products, and include a continuity assessment with respect to the CryoSat-2 LRM mode and cross-comparisons with measurements from other altimeter satellites. A description of generating RDSAR and pseudo-LRM data can be found in the accompanying Algorithm Theoretical Basis Document (ATBD) on RADS RDSAR (Reference Document RD 1).

1.2. Document structure

In this document we validate the RADS RDSAR derived SLA, SWH, and sigma0 at the LRM-SAR transitions over all SAR areas and the St. Helena area ("box") in particular to assess data quality and biases.

In Section 2 we describe the data used, the selected areas and the methods that have been applied to process the data. In Section 3 the validation of the RADS RDSAR L2 altimeter product (PLRM) is performed by zooming in on the LRM-SAR-LRM transitions (near the Island of St. Helena) to compare SLA, SWH, sigma0 and their standard deviations to ensure data quality continuity between SAR and LRM. Global plots of combined LRM and PLRM are investigated, as well as CryoSat-2 SLA, SWH, and sigma0 crossover differences with Jason-1 and Jason-2. And finally in Section 3 we also investigate the long-term evolution of range bias and crossover differences. In Section 4 we summarize the conclusions.

2. Data and method overview

2.1. Selection of data areas

Since the loss of both Jason-1 and Envisat altimeters the role of Cryosat-2 as an operational ocean altimeter has increased significantly, and the need for a global conventional altimeter dataset from Cryosat-2 has become imperative. Figure 2-1 shows the different operating modes for the Cryosat-2 SIRAL altimeter. Most of the time the altimeter works in so-called LRM mode (dark blue areas) and data is available as conventional altimetry (both delay-time LRM and fast delivery FDM). Clearly there are also large patches where the altimeter works in SAR mode (green areas) where data is available as synthetic aperture data with increased along-track resolution, typically with radar returns that are much different from conventional altimetry. However from the so-called FBR data that is available for these areas we can reduce the echoes to an LRM mode product. This process is referred to as reduced SAR or RDSAR, and the deduced LRM data as pseudo-LRM or PLRM. It is especially this product we are interested in and which we will be evaluating in this PVR document. For a detailed description of this reducing process the reader is referred to RD 1. In Figure 2-1 we also see purple areas; here the SIRAL operates in SARIN mode and a 2nd antenna is used to introduce cross-track resolution. This is however not considered in this document.

So, in summary we use all the SAR areas to generate the RDSAR/PLRM products in RADS, by this we generate the global LRM dataset (conventional LRM + PLRM), which subsequently is used to cross-compare with Jason-1 and Jason-2. Also, we have chosen the so-called 'Helena-box', the SAR patch that includes the Island of St. Helena in the South Atlantic Ocean, to look into the transition from conventional LRM to (reduced) SAR to make sure no biases have been introduced. Also in this area not particularly high variability is found and the SWH is close to (global) mean conditions making it suited for unbiased comparisons.

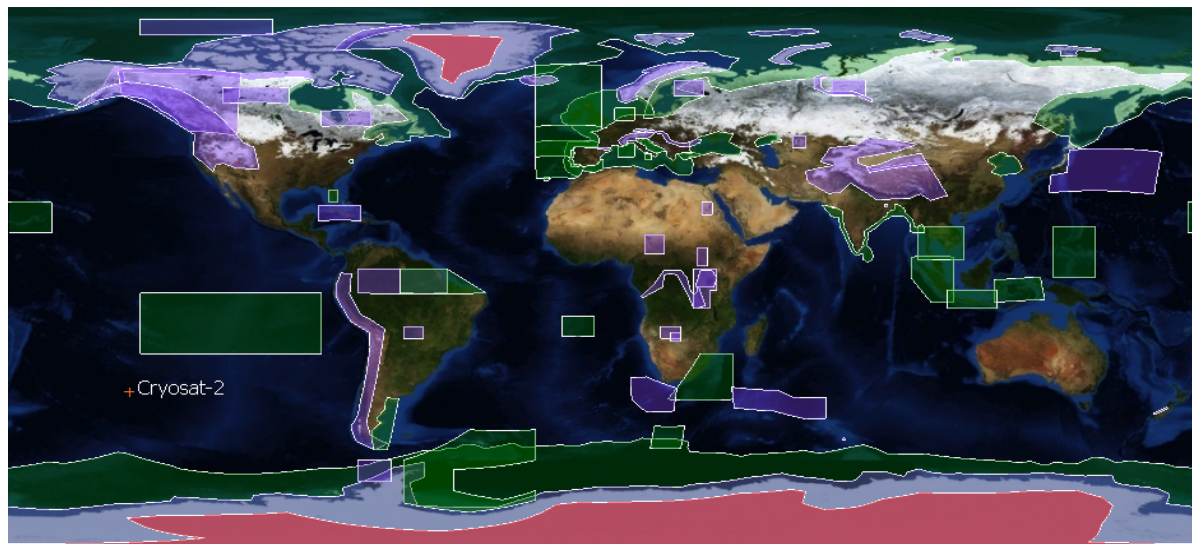


Figure 2-1: The different operating modes of the Cryosat-2 SIRAL altimeter.

2.2. Data processing methodology

2.2.1. Retracking of Cryosat-2 (P)LRM waveforms

The following description is for ESA Baseline B data only. For the conventional LRM we download the FDM and LRM level 1B from ESA on a daily basis, and for the SAR areas we use the FBR Level 1A data. The latter is used to create the pseudo-LRM waveforms as is described in detail in RD 1, and for which Figure 2-2 gives an overview of the process involved.

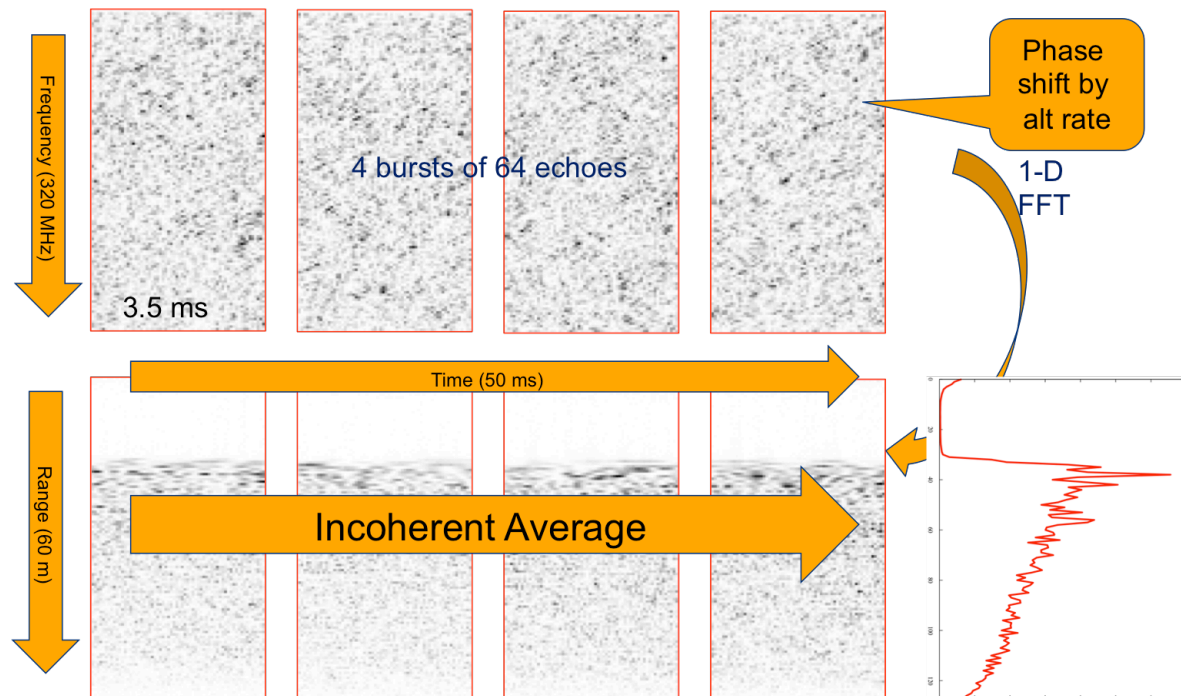


Figure 2-2: Overview of constructing the 20Hz PLRM waveform from 4 bursts of 64 echoes.

Having the LRM and FDM level 1B waveforms and the reconstructed PLRM waveforms we merge LRM and PLRM by retracking the waveforms using the NOAA retracker, an MLE3-type retracker, as developed by Walther Smith from NOAA. This retracker computes the wave height, the backscatter (σ_0) and range (altimeter - sea surface distance). We merge data files that are few to tens of minutes normally into pass and subcycles of 29 days, comparable to what is known as geophysical data records (GDR). The data is then injected into our data base RADS.

2.2.2. Incorporating Cryosat-2 data into RADS

For insertion of the processed data into our database system RADS we convert the timing from international atomic timescale TAI to coordinated universal time UTC (currently a difference of 35 seconds) and create 1-Hz measurements from the 20-Hz measurements. Next to that we apply some updates from our continuous calibration analyses on timing bias and backscatter. For the timing bias we add -4.669112 ms for LRM and +0.520795 ms for PLRM (these are values which we can account for, for which we know the reason), we add another 0.4 ms, which is not yet accounted for but follows from our crossover minimization analyses. Obviously, we adjust the orbital altitude accordingly. Concerning the backscatter, occasional jumps lead to a trend over time; for LRM we add -3.02 dB + 0.22 dB/year, and for PLRM -3.04 dB + 0.27 dB/year (both since 1 May 2011). These values follow from comparing the backscatter with actual wind values over time.

After insertion into RADS we overwrite some of the geophysical corrections from the level 1B data and add common RADS geophysical corrections, in order to have the best available corrections and models and a common reference for all available data in RADS. These include a tailor-made hybrid sea state bias (SSB), the latest mean sea surface (MSS) models (DTU10, CNES-CLS11) and EGM2008 geoid, tides according to FES2004 and GOT4.8, ECMWF and NCEP wet and dry tropospheric correction (from the operational analysed fields), ERA interim wet and dry tropospheric corrections, the GIM and NIC09 ionosphere corrections, the MOG2d dynamic atmospheric correction, a CryoSat-2 reference frame offset of -70.4 cm (constant), and the wind speed computed from the backscatter according to Abdalla's Ku-band wind speed model.

2.2.3. RADS data selection

For our calibration/validation purposes we do the CryoSat-2 data selection directly from RADS and create values for sea level anomaly, SWH and sigma0 by choosing for the CNES GDR-D orbit, ECMWF wet and dry tropospheric corrections, the GIM ionospheric correction, GOT4.8 tides, DTU10 mean sea surface, the earlier mentioned reference frame offset of -70.4cm, the hybrid SSB tailor-made model, and the earlier calibration bias values for Ku backscatter.

In comparison we also extract Jason-1, Jason-2 and Envisat data from RADS for common periods (especially for CryoSat-2 subcycle 29, defined as 11 June 2012 up to 8 July 2012), with common corrections were possible but for instance for the wet tropospheric correction then the value according to the on-board radiometer is used. Also for Jason-1 and Jason-2 instead of the GIM ionosphere correction the one that follows from the dual-frequency correction is used (smoothed). To bring everything in the TOPEX reference frame we also apply different reference frame offsets (biases) to the different altimeters: +44.8 cm for Envisat, +8.8 cm for Jason-1, and -1.8 cm for Jason-2. The same applies to the backscatter altimeters all behaving differently: for Jason-1 and Jason-2 we add -2.4 dB, and for Envisat we apply the value that is supplied on the GDR. Also the SSB for Jason-1 and Jason-2 we keep as supplied on the original GDRs. For CryoSat-2, as we did for Envisat, we have constructed a tailor-made hybrid model. This is shown in Figure 2-3. By fitting an empirical 4-parameter model depending on a constant, wind speed, wind speed squared, and the significant wave height (in short: BM4 model) to the sea level anomalies and blending in the smoothed residuals we obtain a good estimate of the SSB. These models are similar for all altimeters but definitely not identical. The one presented in Figure 2-3 is tailored to the RADS retracked CryoSat-2 baseline B data. The SSB correction in this case roughly comes down to -4% of the SWH.

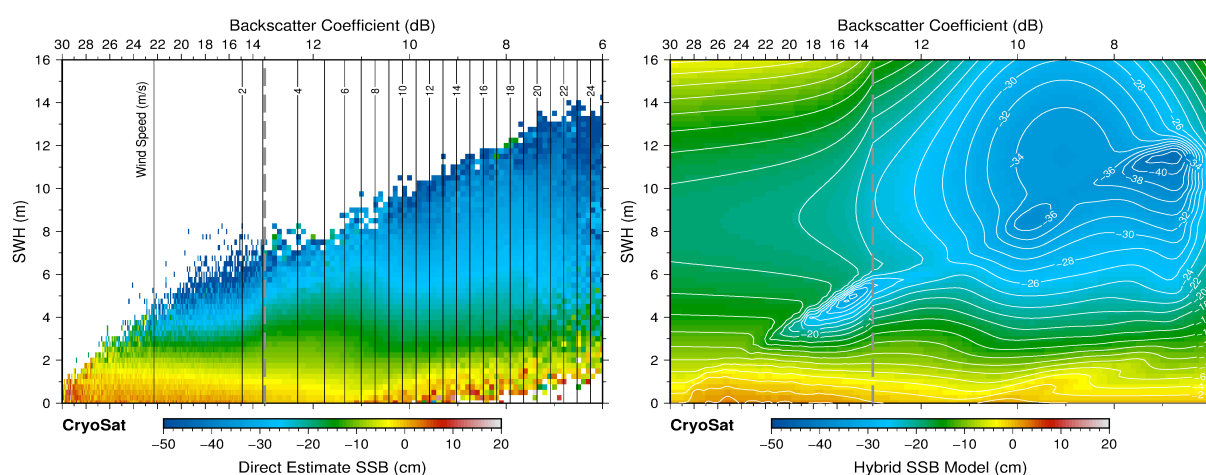


Figure 2-3: Tailor-made hybrid sea state bias model. Left: direct method, sea level anomalies in sigma0-SWH space. Right: Fitted BM4 model with blended in residuals.

3. Validation results and overall assessment

The general objective of this validation exercise is to ensure that the RADS reduced SAR L2 products are consistent and valuable for maintaining the data quality continuity between SAR and LRM modes. Once this is established the combined dataset (LRM + PLRM) can be assessed and inter-compared with other simultaneously operating altimeter missions, and when considered being of the same quality as the Jason missions, they can be employed to enable a better spatial sampling characteristic of the whole (current) altimeter configuration.

In the following, the validation of the RADS RDSAR product (of which the algorithm is described in the accompanying ATBD document) is performed by:

- Analysing the transition of LRM to SAR and back to LRM over the SAR area that contains the island of St. Helena, referred to as Helena box. We investigate the waveform, peakiness, σ_0 , sea surface height anomaly (ssha), significant wave height (swh), and mean quadratic error of the waveform fit (mqe), as well as the sigma's of ssha, swh and σ_0 . We improve the noise and transition statistics by applying the so-called "Jensen-sampling" method. This is especially noticeable for the SWH. To bring the noise level on par with the LRM data we introduce an extra waveform averaging.
- Analysing global plots of combined LRM and PLRM for SLA, SWH and σ_0 to establish any discontinuities globally at all the LRM-SAR and SAR-LRM transitions. Also a direct comparison is made with Jason-1 and Jason-2.
- Analysing crossover mean and RMS differences between CryoSat-2 and Jason-1 and Jason-2.
- Taking a closer look at long-term evolution of range biases and crossover differences.

3.1. LRM - SAR - LRM transition

To improve upon the noise and LRM-SAR-LRM transition statistics we introduce the improved sampling technique of [Jensen, 1999], which is also documented in detail in [Smith and Scharroo, 2014]. In Figure 3-1 it is shown how the sampling of low wave heights is limited by the Nyquist frequency of 160 MHz. When we increase the square magnitude to twice the Nyquist frequency, being 320 MHz, clearly the lower wave heights can be reconstructed more properly.

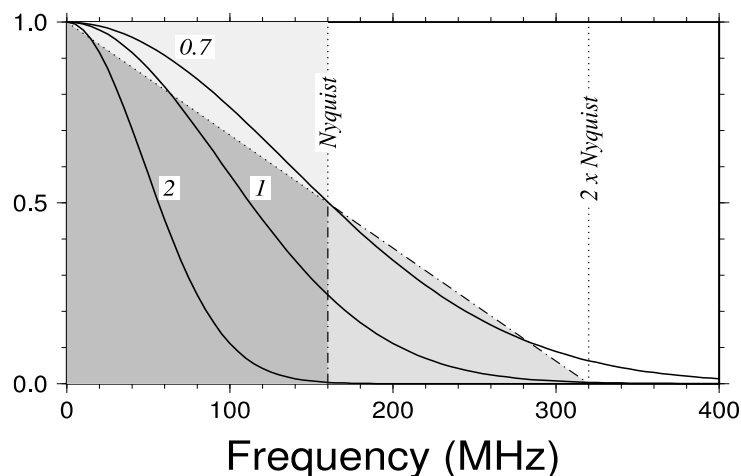


Figure 3-1: Observation of low wave heights limited by Nyquist frequency of 160 Mhz: square magnitude should increase to 320 MHz (2 times Nyquist).

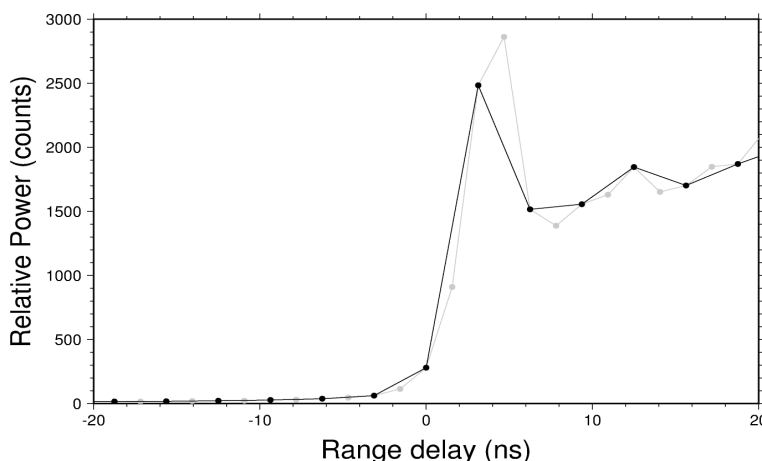


Figure 3-2: Increasing waveform samples from 128 to 256 using technique after Jensen (1999) captures leading edge better.

In Figure 3-2 this is even clearer by showing the retracking for an example waveform. Increasing the waveform samples to 256 doesn't change the values for the original 128 samples, however the extra information changes the waveform shape a bit which leads to a small difference in the midpoint of the leading edge (hence the ssha) and an appreciable change in the steepness of the leading edge (hence the SWH). If we apply this enhanced sampling method the values of both ssha and swh are improved and their noise reduced.

In Figure 3-3 we plotted the along track waveforms and values of peakiness, sigma0, ssha, swh, and mqe, and the sigma's of sigma0, ssha and swh. The part of the track where the altimeter is in SAR mode is indicated by the light blue area. We do not see any discrepancies or discontinuities in the waveforms going from LRM to SAR and back to LRM. Also not in ssha and swh, the noise however for PLRM ssha and SWH (SAR area) is substantially higher, but that was to be expected. To reduce the noise further we employ a waveform averaging combining half of the current waveform and a quarter of the previous and the next waveform. Obviously this will drastically reduce noise in sigma0, swh and ssha: see Figure 3-4. However at the same time it decreases the along-track resolution.

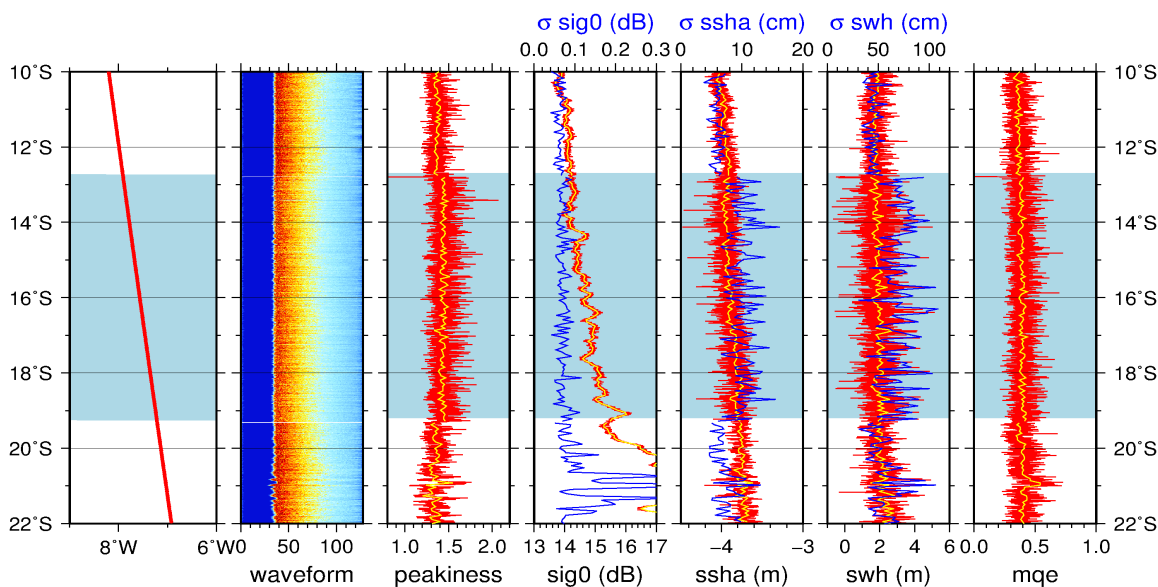


Figure 3-3: Retracking over St. Helana box. Jensen sampling applied.

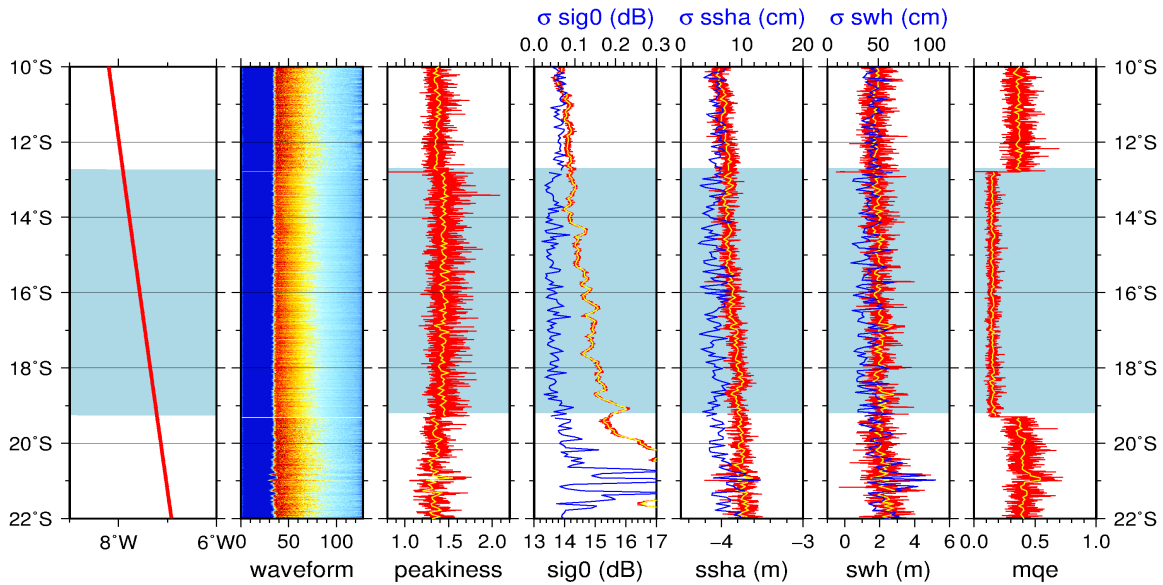


Figure 3-4: Retracking over St. Helena box, noise reduction by $\frac{1}{4} + \frac{1}{2} + \frac{1}{4}$ waveform averaging

For the global LRM + PLRM dataset in RADS we have applied the extra waveform averaging to bring the PLRM statistics on par with the LRM. However, for the dataset that was created for CP40 and which has been used as part of the round-robin validation (WP5000) we omitted this last step to make sure that we stay close to the original data, don't decrease the along-track resolution (not introducing measurements that depend on each other), and to have a dataset that can be compared directly with the CPP RDSAR product (which has no extra waveform averaging applied).

3.2. Global plots of combined LRM and PLRM

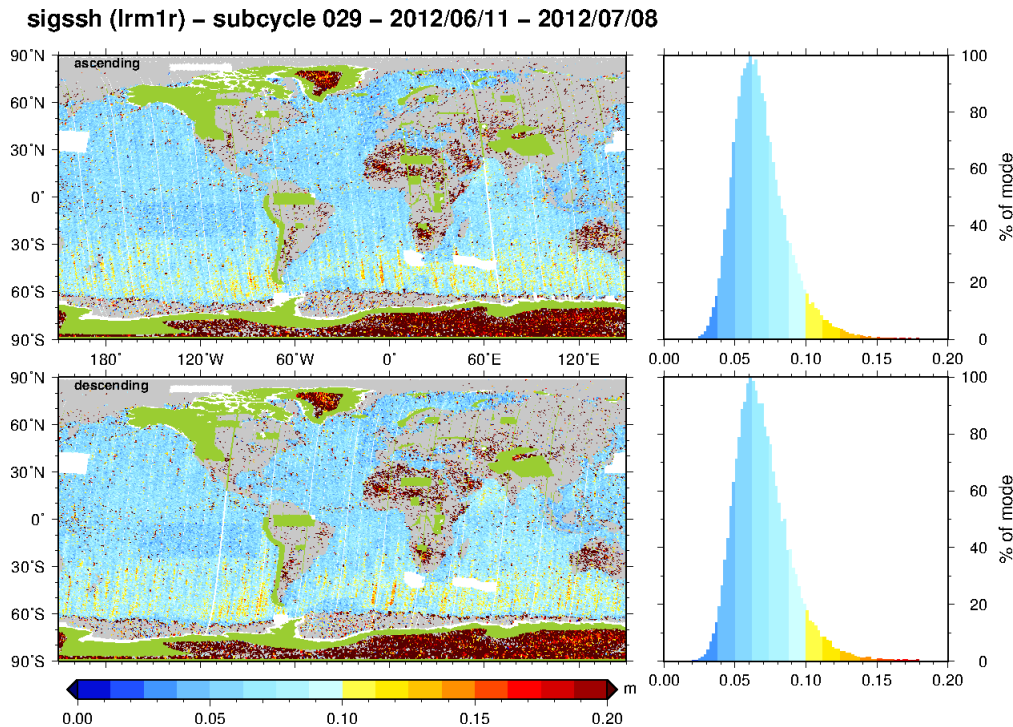


Figure 3-5: Cryosat-2 standard deviation in sea level: LRM and PLRM combined.

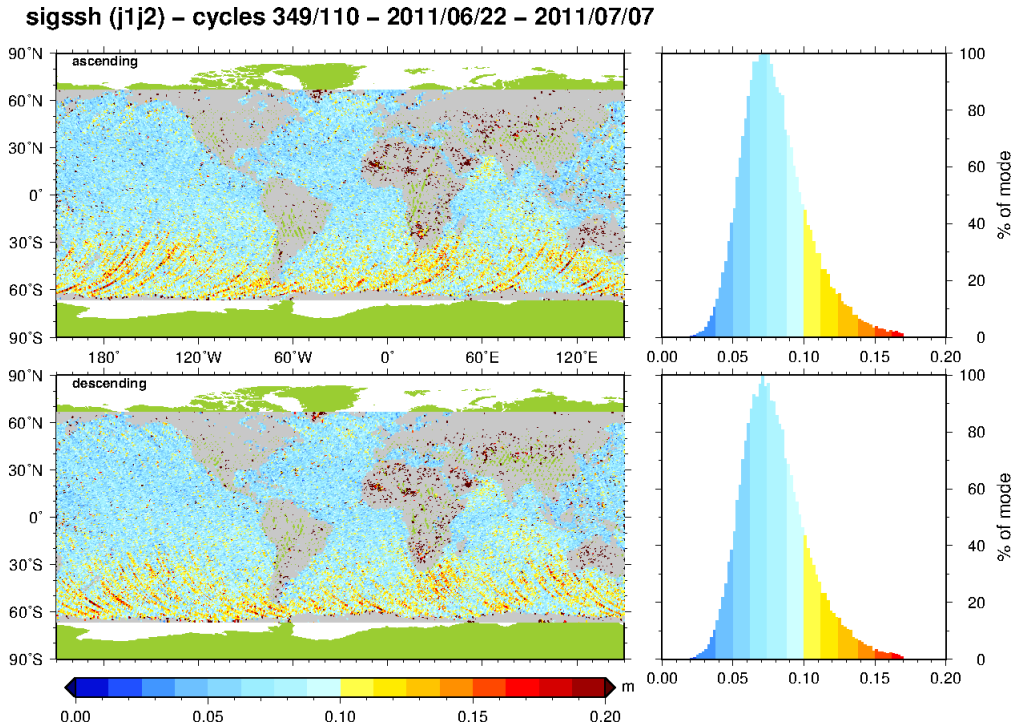


Figure 3-6: Jason-1/2 standard deviation in sea level.

In Figure 3-5 and Figure 3-6 the standard deviation of the sea level anomaly has been plotted globally for CryoSat-2 combined LRM and PLRM and Jason-1/2 respectively. This roughly covers the period 11 June 2011 - 8 July 2011 (CryoSat-2 subcycle 29). For Jason cycles have been chosen that lie within this timeframe. Clearly, the standard deviation for the CryoSat-2 SLA is on par with the Jason-1/2 data, showing comparable structures and averaging around 6 cm versus 7 cm for Jason. That it is slightly lower must be due to the incorporation of the SAR patches where the noise was artificially brought down by the applied waveform averaging mentioned in Section 3.1.

In Figure 3-7 we plotted the retracked SLA standard deviation (σ_{ssh}) versus the retracked SWH. We see expected behaviour and similar for LRM and PLRM. Obviously the dependency or correlation (tilt in the regression line) is stronger for LRM but that is because the LRM also covers the areas with larger wave heights. The peak in number of points is the same for both: around 5 cm standard deviation for 2-m wave height.

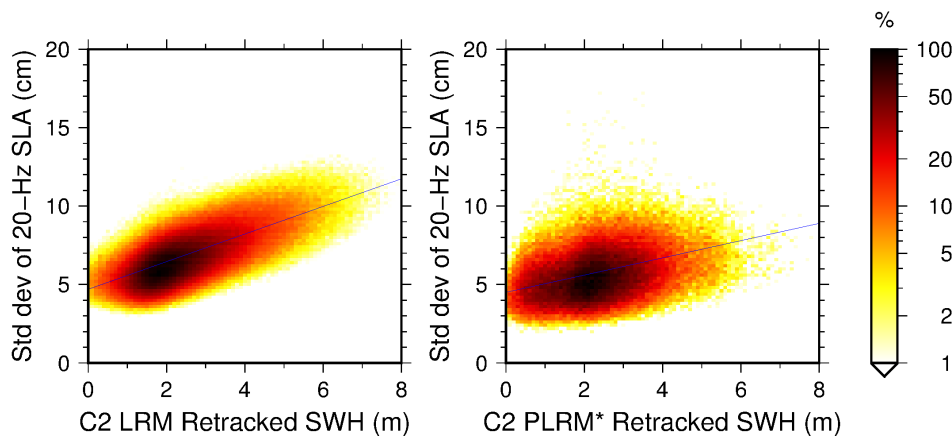


Figure 3-7: Standard deviation as function of SWH for LRM (left) and PLRM (right).

In Figure 3-8 the global maps of LRM SLA and PLRM SLA have been combined and plotted. In the top panel the ascending tracks and bottom panel the descending tracks. We can see a very good general agreement between LRM and RDSAR data over the globe and notably at the transition between LRM and SAR modes: we don't see any discontinuity. Reduced SAR retrieval results are found to be very consistent with the ocean structures as observed by the LRM. This can also be shown when zooming in to the different transition zones: see Figure 3-9. This makes the complete CryoSat-2 LRM+PLRM data set very suited for complementing the other operational satellites Jason-2 and SARAL to improve the sampling of mesoscale ocean dynamics.

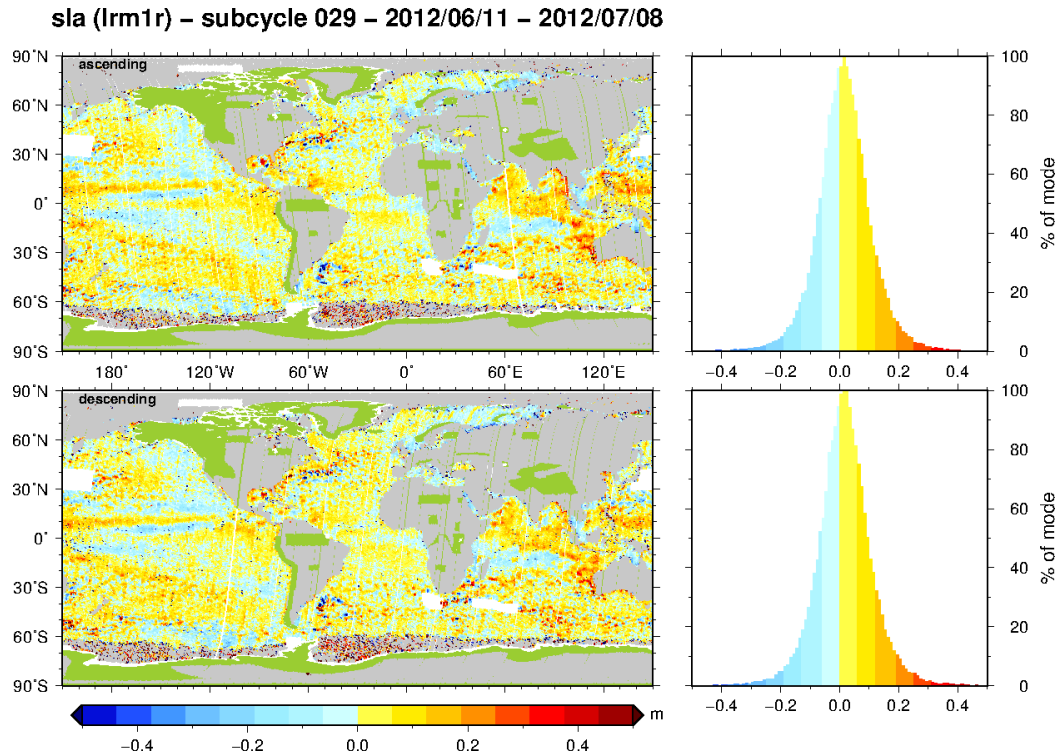


Figure 3-8: CryoSat-2 SLA from PLRM and LRM combined.

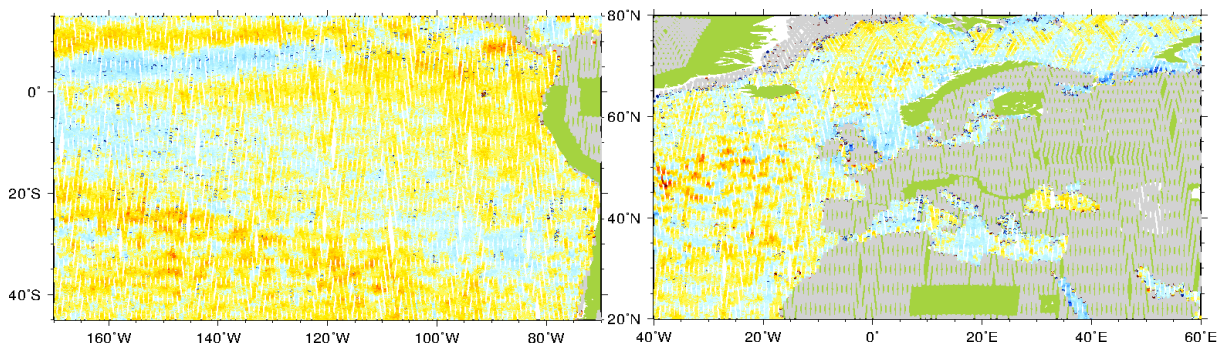


Figure 3-9: SLA zoomed in on central East Pacific and Northeast Atlantic.

In addition to the global SLA we also plotted the combined LRM and PLRM SWH in Figure 3-10 and sigma0 in Figure 3-11, and come to the same conclusion that the transitions between LRM and SAR are visually non-existent and therefore seamless.

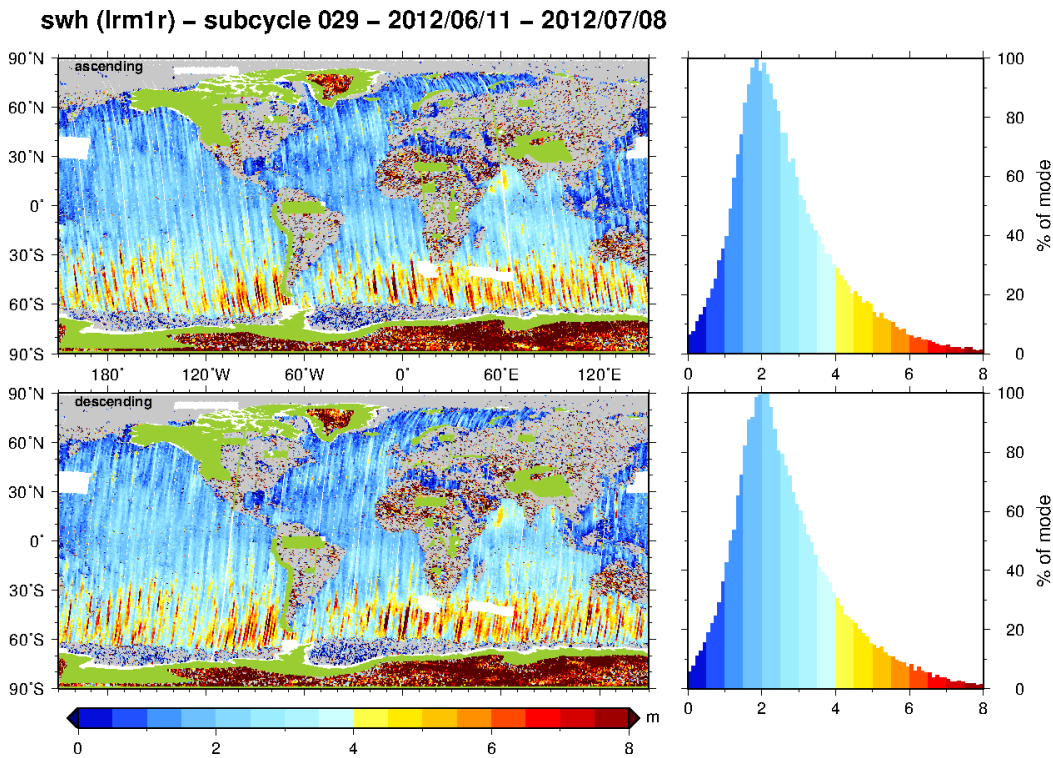


Figure 3-10: CryoSat-2 SWH from PLRM and LRM combined.

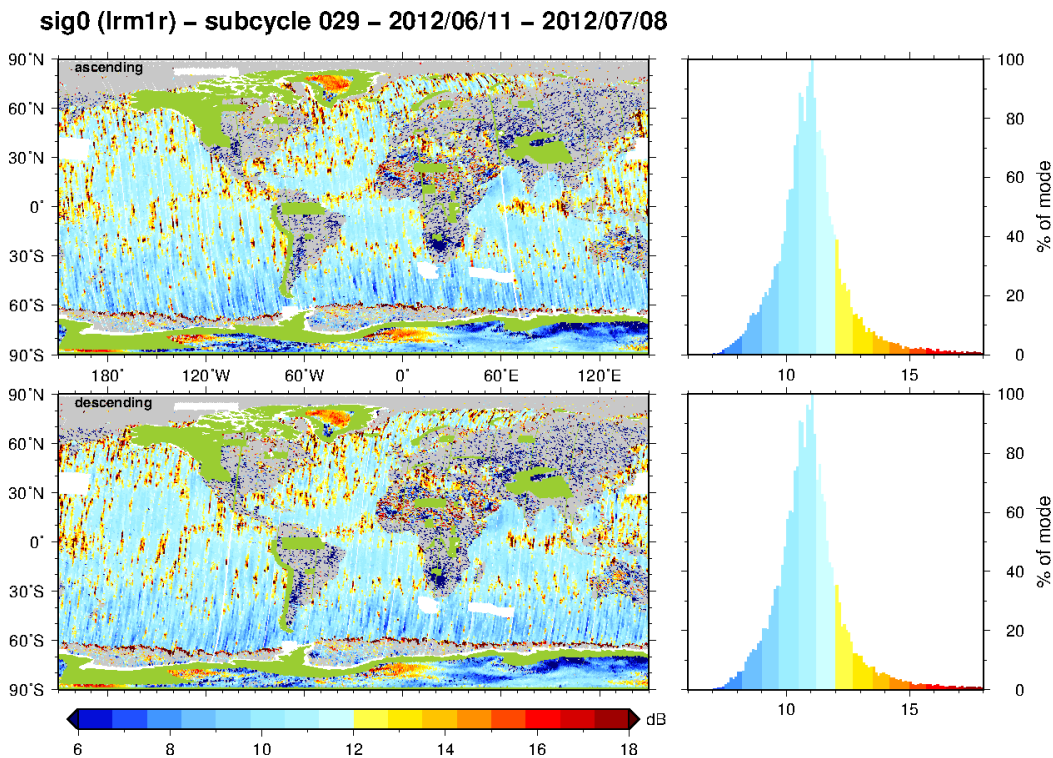


Figure 3-11: CryoSat sigma0 from PLRM and LRM combined.

3.3. Crossover differences

Another way of assessing data quality and calibrating the data is to analyse the crossover statistics and plot geographical maps of the crossovers. In Figure 3-12 and Figure 3-13 scatterplots are shown for SWH and sigma0 comparing our retracked CryoSat-2 data and Jason-2 data. This comparison is done at identical locations (crossover locations between the two satellite tracks) and making sure that the data are not further apart than 5 days. Clearly we cannot directly compare CryoSat-2 LRM with CryoSat-2 PLRM because no crossovers exist as the satellite is either in LRM mode or SAR mode (in fact, some crossovers exist between ascending and descending where one is in SAR mode and the other in LRM mode but the number is just too few to draw any useful conclusions). Both SWH and sigma0 compare very well; the regression line is close to the identity line (45°). The PLRM backscatter seems a bit more spread than the Jason-2 backscatter, which has to be looked into but falls outside the scope of this document.

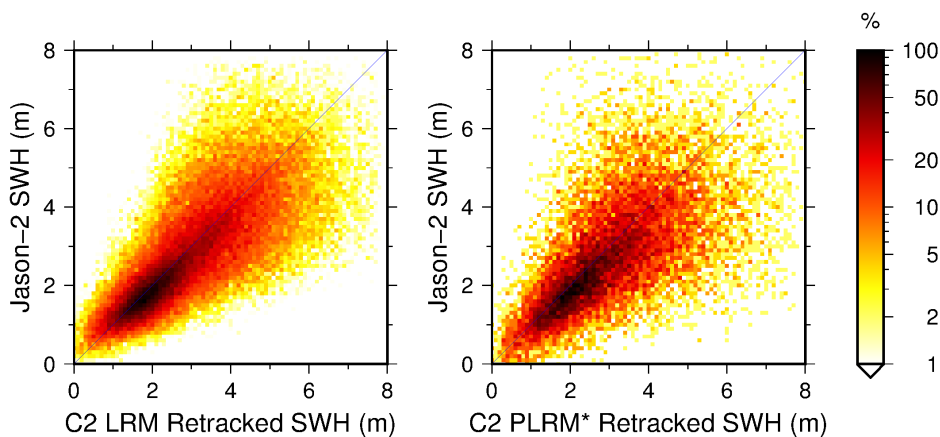


Figure 3-12: Scatterplot CryoSat-2 SWH LRM (left) and PLRM (right) with Jason-2 SWH at crossovers $\Delta t < 5$ days.

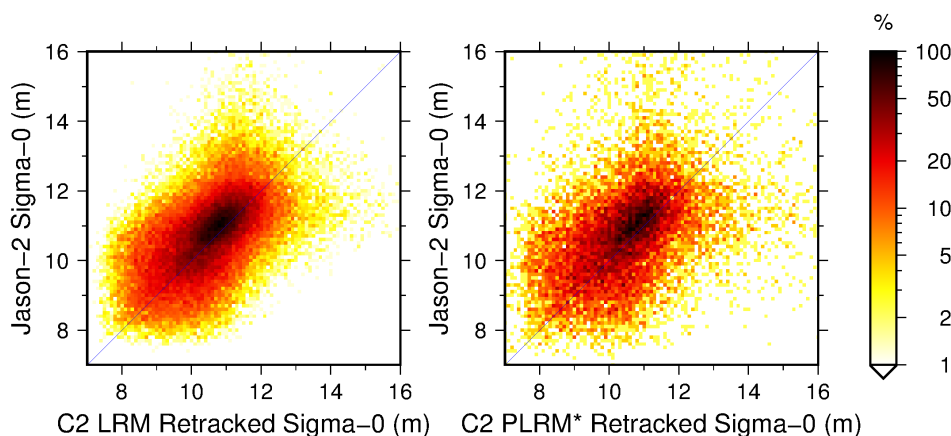


Figure 3-13: Scatterplot CryoSat-2 sigma0 LRM (left) and PLRM (right) with Jason-2 sigma0 at crossovers $\Delta t < 5$ days.

In Figure 3-14 the global plots are shown for the crossover differences between the combined LRM and PLRM CryoSat-2 sea level (SLA) data and Jason-1 and Jason-2 SLA data. For comparison also the crossover differences between Jason-1 and Jason-2 are plotted. Crossovers are collected that lie within 5 days of each other. The RMS of the crossover differences show the usual enhanced variability in the vicinity of the western boundary currents; all the maps look very much the same showing that the CryoSat-2 data is as good as the data from the Jason altimeters. The statistics summarized in Table 3-1 underpin this statement; the standard deviation for CryoSat-2 LRM crossovers with Jason-1/2 is 5.3 cm, and for Jason-1 crossovers with Jason-2 5.2 cm which is practically the same. For PLRM the 5.6 cm is slightly worse but still in the same league. The mean of crossovers is close to zero in all cases, we do see a geographical (zonal) dependence in the crossover differences with Jason-2 for both CryoSat-2 and Jason-1. This dependency disappears when we inter-compare CryoSat-2 and Jason-1.

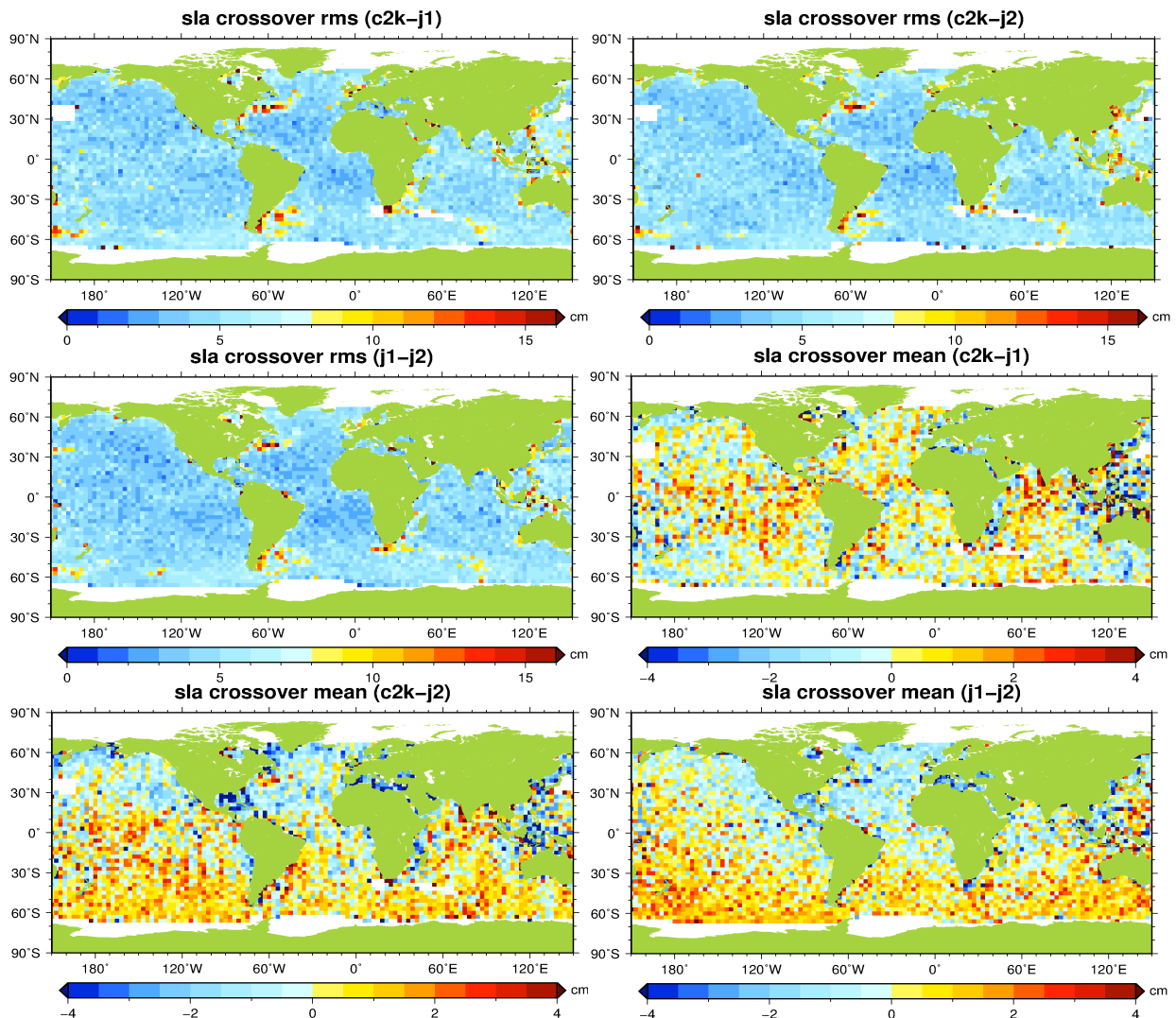


Figure 3-14: CryoSat-2 retracked sea level (SLA) crossover differences. From left to right and from top to bottom: RMS with Jason-1, Jason-2, and Jason-1 with Jason-2, and mean with Jason-1, Jason-2, and Jason-1 with Jason-2.

Table 3-1: Crossover statistics for CryoSat-2 (CS) retracked SLA, SWH and sigma0 with the Jason-1 data (JS1) and Jason-2 data (JS2).

Crossover combination	SLA Mean [cm]	SLA Std [cm]	SWH Mean [m]	SWH Std [m]	Sig0 Mean [dB]	Sig0 Std [dB]
CSLRM-JS1	-0.26	5.32	+0.17	1.21	-0.53	1.78
CSLRM-JS2	+0.11	5.26	+0.15	1.20	-0.21	1.76
CSPLRM-JS1	+0.04	5.55	+0.26	1.27	-0.55	1.95
CSPLRM-JS2	+0.20	5.56	+0.26	1.26	-0.23	2.00
JS1-JS2	+0.32	5.18	-0.13	1.20	+0.32	1.74

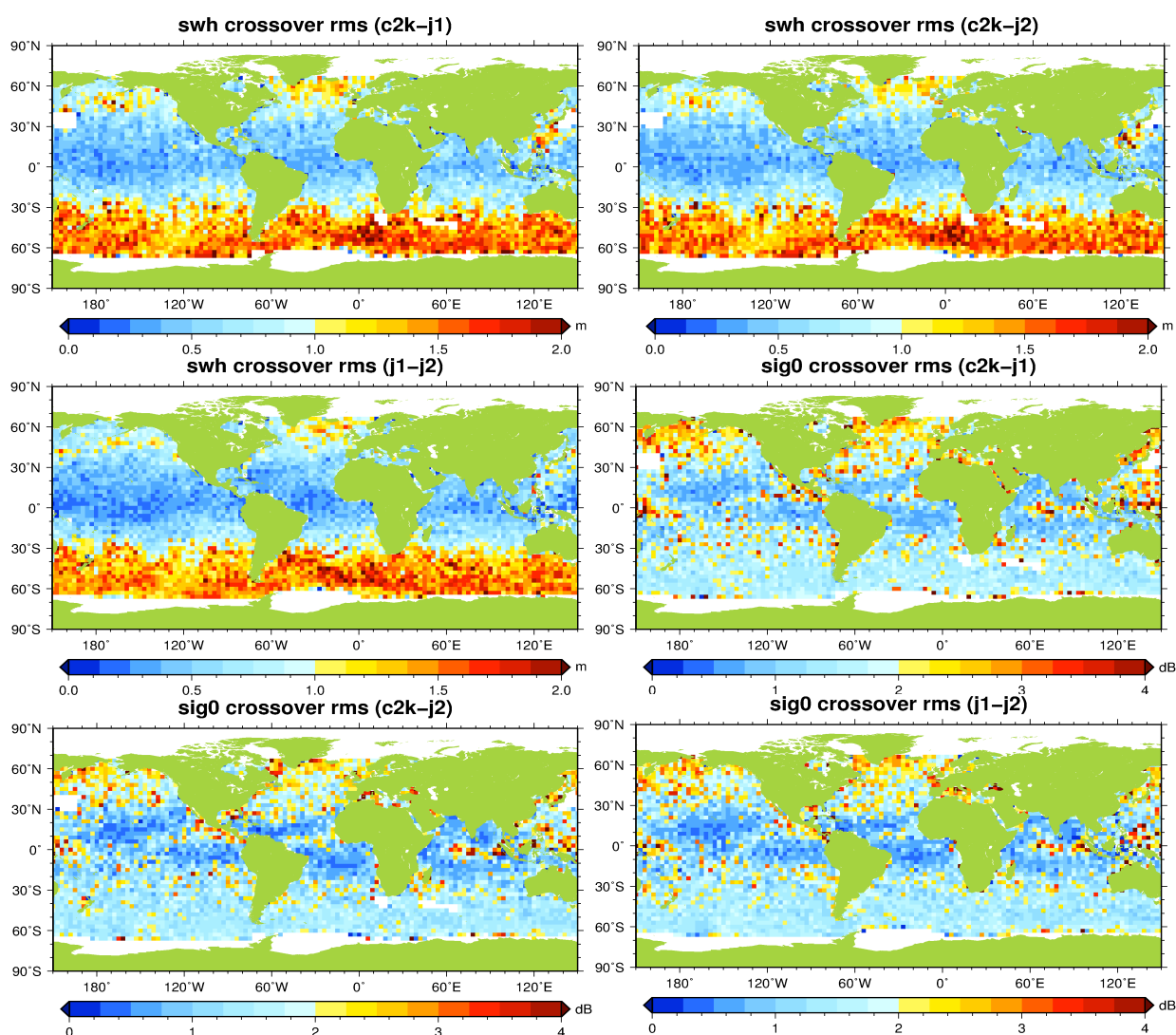


Figure 3-15: CryoSat-2 retracked SWH and sigma0 crossover differences. From left to right and from top to bottom: RMS SWH with Jason-1, Jason-2, and Jason-1 with Jason-2, and RMS sigma0 with Jason-1, Jason-2, and Jason-1 with Jason-2.

For completeness sake we also show in Figure 3-15 global plots for the crossover differences between the combined LRM and PLRM CryoSat-2 significant wave height (SWH) data and Jason-1 and Jason-2 SWH data, and the CryoSat-2 sigma0 (sig0) data and Jason-1 and Jason-2 sigma0 data. For comparison also the crossover differences between Jason-1 and Jason-2 are plotted. Again we collected crossovers within a timeframe of 5 days. The accompanying statistics can also be found in Table 3-1. Most standard deviations (rms) of the crossover differences are comparable only the backscatter for the PLRM seems somewhat higher than that for LRM and Jason-1/2. In the mean the only noticeable fact is that CryoSat-2 LRM SWH is 15cm higher than the reference missions, and PLRM SWH is about 20 cm higher. The conclusion is that the combined CryoSat-2 LRM and PLRM data set is of comparable quality as Jason-1 and Jason-2, not just for SLA but also for SWH and sigma0.

3.4. Long-term evolution of range bias and crossover difference

Analysing the daily mean of sea level anomaly, significant wave height and sigma0 and their crossover values we can draw some conclusions about the stability of the biases and their values. For this we refer to Figure 3-16 for the SLA, Figure 3-17 for the SWH, and Figure 3-18 for sigma0.

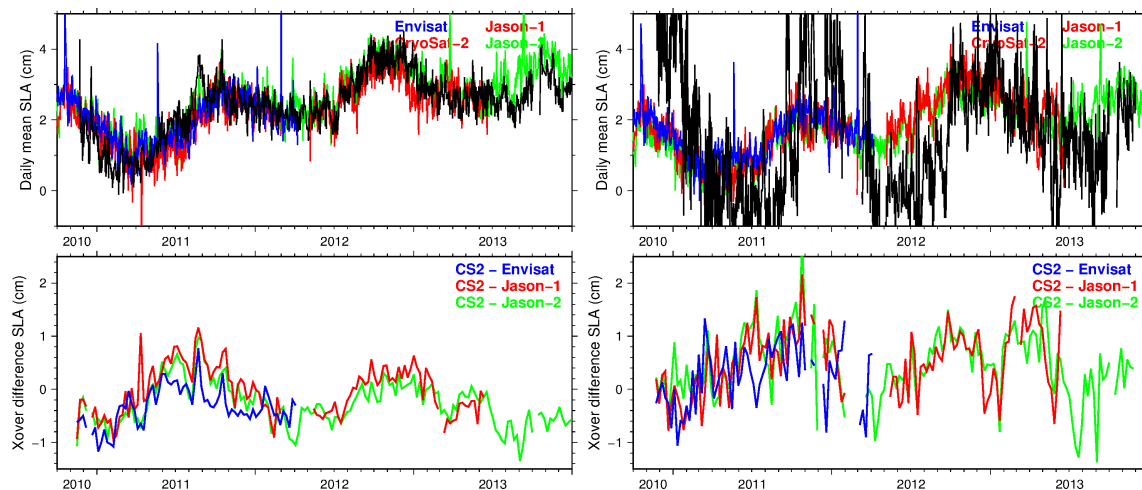


Figure 3-16: Time series of sea level anomaly (top) and SLA single-satellite crossover differences (bottom), Cryosat-2 LRM only (left) and PLRM only (right).

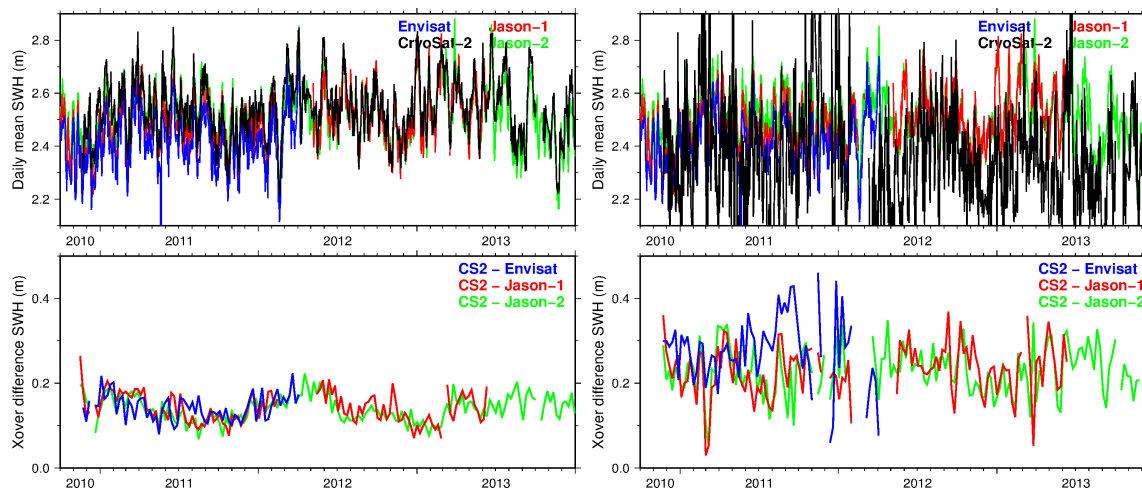


Figure 3-17: Time series of significant wave height (top) and SWH single-satellite crossover differences (bottom), Cryosat-2 LRM only (left) and PLRM only (right).

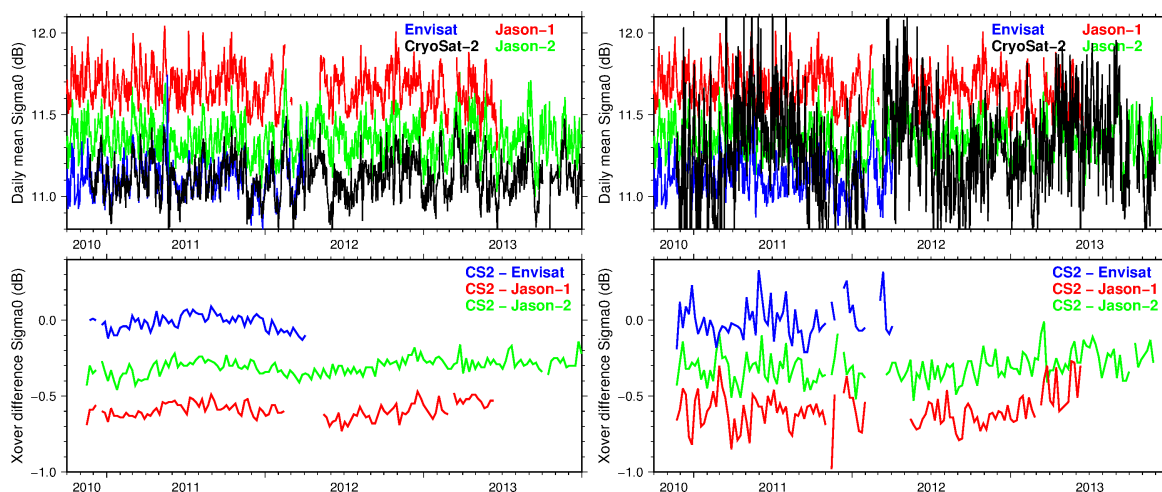


Figure 3-18: Time series of sigma0 (top) and sigma0 single-satellite crossover differences (bottom), Cryosat-2 LRM only (left) and PLRM only (right).

In the top panel you find the time series of the daily mean and in the bottom panel the time series of the mean crossover difference (ascending minus descending). Concerning the SLA biases they are a few mm at most comparing CryoSat-2, Envisat, Jason-1 and Jason-2 confirming the proper reference frame offsets used for the different satellites. This is true when we choose also the ECMWF wet troposphere correction and GIM ionosphere correction (so basically all satellites the exact same corrections). The global mean shows the expected seasonal behaviour, whereas we see a 500-day cycle in the crossover evolution, which is related to the beta-angle of the orbit (or the satellite's exposure to direct sunlight). Concerning the bias in SWH we notice (Figure 3-17) a little apparent bias in the global mean. The SWH crossovers show that CryoSat-2 is biased high by approximately 15 cm for LRM and 20 cm for PLRM. The seasonal behaviour is apparent in the daily global mean but very small in the crossover differences. Lastly, concerning the biases in the backscatter (sigma0), we see for both LRM and PLRM no bias with Envisat, with Jason-1 a bias of -0.6 dB, and with Jason-2 of -0.3 dB. The seasonal variation in daily mean and crossover difference is very small, the fluctuations ("noise") in the PLRM is somewhat higher than in the LRM results.

4. Conclusion

The continuity assessment between RADS LRM and RADS RDSAR data has been performed globally in the open ocean and particularly in the so-called St. Helena box. The results show good agreement at both sides (LRM and SAR) of the transitions, with no significant bias in SLA and SWH between both operating modes. This can be seen for one track in the St. Helena box but is also very obvious from global plots of SLA, SWH and sigma0 when the RADS LRM and PLRM are combined. Obviously the 1Hz noise on SLA/SWH RDSAR data is higher than the LRM one, as expected, but typically better than the theoretical $\sqrt{3}$ since more pulses contribute to the pulse de-correlation. Improvements in noise and actual values for SLA and SWH have been obtained by increasing the waveform sampling (doubling the Nyquist frequency) and by an additional scheme of waveform averaging.

Biases found at the continuity between RDSAR estimates and LRM ones are not significant: they all fall within the same range as the (increased) noise of the RDSAR data product.

Concerning our combined LRM and PLRM RADS product we applied a reference frame offset to the CryoSat-2 SLA data of -70.4 cm to put it in the TOPEX reference frame. For Envisat we apply $+44.8$ cm, for Jason-1 $+8.8$ cm, and for Jason-2 -1.8 cm, in order to have all altimeter data in the same reference frame. Clearly this is important when calculating sea level change and combining data from different altimeter satellites. Figure 4-1 shows how well CryoSat-2 fits in the curve of global mean sea level evolution, following the curves by Jason-1/2 and Envisat, and even better the SARAL curve (recent Ka-band altimeter) because of the high-inclination orbit.

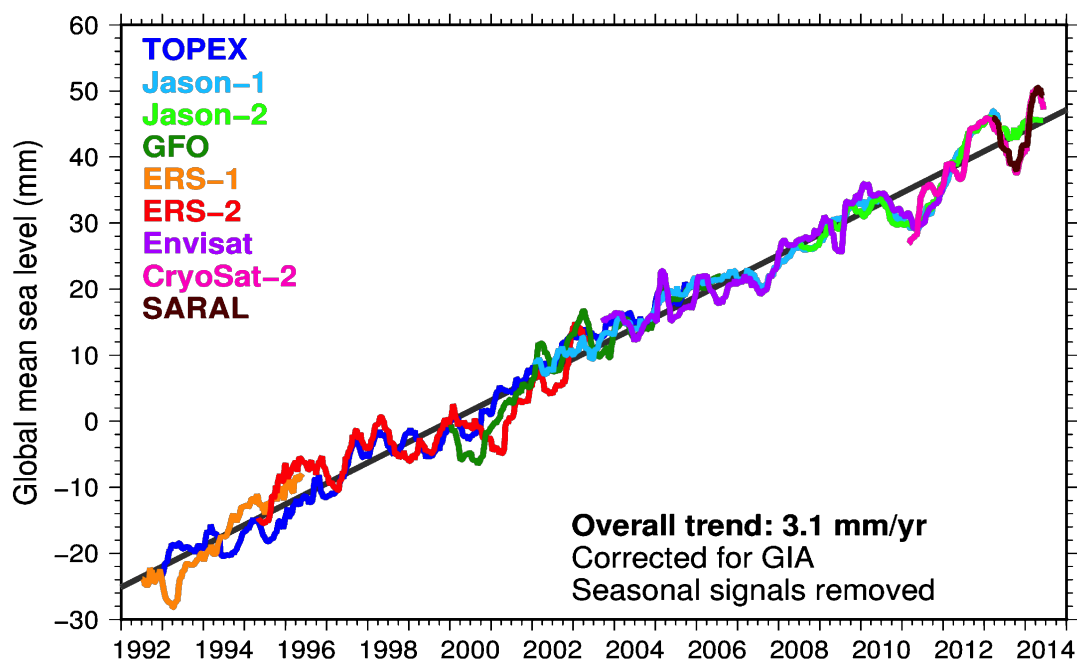


Figure 4-1: Evolution of global mean sea level including all historic altimeter data available in RADS. The CryoSat-2 result seamlessly fit the earlier and simultaneous data.

The remaining bias for CryoSat-2 after applying this overall reference frame offset is just a few mm fluctuation, showing some beta-angle related variation. The CryoSat-2 SWH data seem to be biased high by about 15cm for LRM and 20 cm for PLRM. And, the CryoSat-2 sigma0 data or backscatter coefficient is adjusted for drift and an approximate -3.0 dB bias, whereas Jason-1 and Jason-2 are adjusted by -2.4 dB. Remaining bias after these adjustments in CryoSat-2 data with Envisat is 0.0 dB, with Jason-1 -0.6 dB, and with Jason-2 -0.3 dB. The variations around these means are very small, showing some seasonal behaviour.

Concerning the retracked LRM L1B data we can conclude that the retracking can be performed with MLE3 with a priori off-nadir angle from star-tracker information, and that these retracked L1B data show excellent quality. The crossovers with Jason-1/2 show sea level variance only slightly higher than crossovers between Jason1/2, due to the lack of radiometer and dual frequency altimeter data (that's why we needed models and external data for the wet troposphere and ionosphere corrections).

Concerning the retracked pseudo-LRM (PLRM) data we conclude that reducing SAR and determining PLRM data is possible by stacking the SAR echoes, doubling the number of bins (to 256), smoothing the waveforms by combing waveforms with previous and next ones, and by applying the same retracking as used for the LRM L1B data. In this manner we get no apparent bias with the LRM data. We initially do get higher levels of 20Hz noise but that can be reduced applying waveform smoothing. We conclude that the PLRM data quality is on par with the quality of the LRM data. We are convinced that the RADS reduced SAR L2 products are a good LRM-reference during SAR-mode maintaining the continuity with the LRM mode data and allowing the assessment of the in-orbit performances of the SAR mode data.

5. References

- [Jensen, 1999]: J.R. Jensen, “*Radar altimeter gate tracking: Theory and extension*”, IEEE Trans. Geosci. Rem. Sens., 37(2), 651-658, 1999.
- [Scharroo et al, 2012a]: R. Scharroo, W.H.F. Smith, and M.C. Naeije, “*Validation of CryoSat test data set over open oceans (LRM and FDM, Level 1 and 2)*”, Tech. rep., Altimetrics LLC, 2012.
- [Scharroo et al, 2012b]: R. Scharroo, W.H.F. Smith, and M.C. Naeije, “*Updated validation of CryoSat test data set over open oceans (LRM and FDM, Level 1 and 2)*”, Tech. rep., Altimetrics LLC, 2012.
- [Scharroo et al, 2012c]: R. Scharroo, W.H.F. Smith, and M.C. Naeije, “*Re-updated validation of CryoSat test data set over open oceans (LRM and FDM, Level 1 and 2)*”, Tech. rep., Altimetrics LLC, 2012.
- [Scharroo et al, 2012d]: R. Scharroo, W.H.F. Smith, J.L. Lillibridge, and E.W. Leuliette, “*Cal/Val of combined conventional and reduced SAR mode data over oceans and in the coastal regime*”, presented at Sixth Coastal Altimetry Workshop, Riva del Garda, Italy, 20-21 September, 2012.
- [Scharroo et al, 2012e]: R. Scharroo, W.H.F. Smith, J.L. Lillibridge, and E.W. Leuliette, “*Global Cal/Val of CryoSat-2 LRM and SAR data over oceans*”, presented at the Ocean Science Topography Science Team Meeting, Venice, Italy, 27-29 September, 2012.
- [Scharroo et al, 2013a]: R. Scharroo, W.H.F. Smith, E.W. Leuliette, and J.L. Lillibridge, “*The performance of CryoSat-2 as an ocean altimeter*”, in Proc. of the CryoSat-2 Third User Workshop, Dresden, 12-14 March 2013, Eur. Space Agency Spec. Publ, ESA SP-717, p. 5 pp, 2013.
- [Scharroo et al, 2013b]: R. Scharroo, W.H.F. Smith, E.W. Leuliette, and J.L. Lillibridge, “*CryoSat-2: The other ocean altimeter*”, ESA Living Planet Symposium, Edinburgh, Scotland, 9-13 September, 2013.
- [Smith and Scharroo, 2014]: W.H.F. Smith, and R. Scharroo, *Waveform aliasing in satellite radar altimetry*, IEEE Trans. Geosci. Rem. Sens., doi:10.1109/TGRS.2014.2331193, in press, 2014.